Sedimentation of an elliptical object in a two-dimensional foam

I.T. Davies, S.J. Cox[1]

Institute of Mathematics and Physics, Aberystwyth University, Ceredigion SY23 3BZ, UK

Abstract

The sedimentation of an elliptical object in a dry two-dimensional, monodisperse foam is simulated. The calculations are quasi-static, allowing the identification and separation of the elastic, plastic and viscous response of the foam to the motion. In addition to its weight, the forces on the ellipse are due to the network of soap films and the pressures in the bubbles. These give rise to non-zero torque, lift and drag forces, causing the motion of the ellipse to deviate from a vertical path. Highly-stretched films are formed in the wake of the ellipse and asymmetry in the flow field, with bubbles moving from the front to the back of the ellipse along only one side, causes it to rotate from a metastable state with its major axis perpendicular to gravity into a stable orientation with its major axis parallel to the direction of gravity. When the orientation is intermediate between these two limits, there is a significant lift force which causes the ellipse to move laterally. A larger, more eccentric, ellipse rotates more quickly.

Key words: foam, ellipse, sedimentation

[1]Corresponding author. Email: foams@aber.ac.uk. Tel: +44 1970 622764. Fax: +44 1970 622826.

1. Introduction

Liquid and solid foams are familiar materials that are used in a variety of domestic products. They are also important in many industrial processes such as mineral separation and enhanced oil recovery [1, 2, 3]. Aqueous foams are complex fluids, in the sense that their response to applied stress is highly non-linear: they exhibit elastic, plastic and viscous characteristics. At low stresses, a foam behaves as an elastic solid. Increasing the applied stress results in T1 topological changes, plastic events during which bubbles rearrange and swap neighbours, giving rise to a yield stress. Increasing the applied stress above a foam's yield stress leads to viscous liquid-like behaviour [4].

Liquid foams provide a prototypical complex fluid with which it is possible to work at the scale of constituent particles (bubbles) of the order of millimetres, instead of the usual microscopic scale. Here, the complex nature of foams is studied by looking at the sedimentation of an elliptical object descending under its own weight through a two-dimensional (2D) foam, a variation of the classical Stokes experiment [5].

It has been known since the 1960s [6, 7] that the fluidized region surrounding a long object falling in a yield stress fluid is highly dependent on its orientation. Brunn [8] showed that only two orientations are stable: with the long (or major) axis parallel or perpendicular to the direction of gravity. Rod-like particles descending through viscoelastic fluids [9] and other long objects in fluids with high elasticity [10, 11] turn so that their long axis is *parallel* to gravity, in contrast to the case of purely viscous Newtonian fluids [12], as a result of compressive normal forces.

Joseph and Liu [13] propose that the tilt angle of a long body falling in a viscoelastic liquid is determined by the competition between viscous, viscoelastic and inertial effects. Their 3D experiments on the settling of a cylindrical rod in a viscoelastic fluid showed that for light particles the viscoelasticity of the fluid dominates and turns the long body such that its major axis is parallel to gravity. In contrast, when a heavy particle was allowed to settle minimal rotation of the object was seen.

Probing the response of a foam by looking at its flow past circular or spherical objects is becoming a standard tool [see e.g. 14], but the use of asymmetric objects such as an ellipse is unusual, despite the possibility of further exploring a foams' complex response. A notable exception is the work of Dollet et al. [15], who studied the 2D flow of foam past a freely rotating ellipse (and later an aerofoil [16]) with a fixed centrepoint. Their experiment consisted of a monolayer of equal-area bubbles bounded between a glass plate and a water sub-phase moving at constant velocity. Attaching the ellipse's centre to a thin elastic fibre enabled the measurement of the drag and lift forces as well as the torque exerted on the object. The torque caused the ellipse to rotate so that its major axis became parallel to the direction of foam flow, and the angular velocity of the ellipse was greatest when the angle between its major axis and the direction of the

flow was between 15° and 40°.

Our simulations, described below, are inviscid, and therefore allow us to distinguish the effects of viscosity from the elasticity of the foam during sedimentation. Previously we showed, using a similar method, that the stable configuration for two discs falling through a dry 2D foam was such that they were one above the other, provided they started within a critical distance of each other of the order of a few bubble diameters. That work lacks experimental confirmation. Here, we simulate the rotation of a single fixed *elliptical* object in a foam flow, validate this against experiment [15], and then use the simulations to probe the response of a dry 2D foam to the *sedimentation* of an elliptical object. We systematically vary control parameters including the area and eccentricity of the ellipse and separate the contributions of bubble pressures and the film network.

2. Method

We use a quasi-static model, implemented in the Surface Evolver [17], in which the motion of the object in the foam is assumed to be so slow that viscous effects do not change the structure of the foam.

The initial foam structure is created from a Voronoi construction [18] based upon randomly distributed seed points. We use the Surface Evolver in a "circular arc" mode, in which each soap film is represented by a circular arc, providing high accuracy and computational efficiency. We set all bubble areas A_b to be equal (monodisperse foam): the drag forces depend weakly upon the area disorder [19], and we expect the same to be true of the torque.

In a real foam, a T1 event occurs whenever a film shrinks to zero length; the effect of liquid is to cause the vertices to swell and the films between them to shrink. To mimic this effect in our dry foam model, we allow T1s when the films have a finite length representing (twice) the size of the real vertices [20]. That is, we introduce a finite cut-off film length l_c which increases with effective liquid fraction and below which a T1 is triggered. This cut-off length is kept constant and small here, representing a dry foam: we choose $l_c = 3.6 \times 10^{-3}$, appropriate to a liquid fraction of $\phi_l = 4 \times 10^{-3}$. The structure is equilibrated by minimizing the total film length (the film tension, equal to twice the interface tension γ, is set equal to one throughout) subject to the area constraints, allowing T1s when required.

The foam is embedded in a channel, and the top and bottom of the channel are connected by a periodic boundary condition [21]. The channel has length $L = 1$ and width $W = 0.47$ and contains 600 bubbles so that the walls are roughly 15 bubbles apart. Vertices that touch the ellipse are free to slip. We then convert one bubble into an elliptical object with centre (x_0, y_0), eccentricity e_c and area A_e, ensuring that

the bubble's vertices satisfy the constraint:

$$\frac{1}{e_c^2}\left[(y-y_0)\cos\phi-(x-x_0)\sin\phi\right]^2+e_c^2\left[(y-y_0)\sin\phi+(x-x_0)\cos\phi\right]^2=A_e/\pi, \tag{1}$$

where ϕ denotes the angle at which its major axis is oriented relative to the horizontal x-axis. See figure 1.

[Figure 1 here]

We perform two types of simulations. Firstly, we cause the foam in the channel to flow in the positive y direction by incrementing the position of a line of films using the method described in [22], employing a slip boundary condition on the channel walls. The centre of the ellipse is fixed in the centre of the foam channel, $x_0 = 0.235, y_0 = 0.5$. We measure the forces on the ellipse, as described below, and allow it to rotate a small amount in response to the torque before finding a new local equilibrium of the foam. Secondly, we allow the ellipse to sediment by placing it at the top of the centre of the foam channel, far enough from the channel walls that attraction/repulsion from the wall can be neglected [14, 19]. In this case the vertices at which films meet the walls of the channel are fixed after the first equilibration, so that a no-slip boundary condition is maintained there. We measure the forces on the ellipse, now including its weight, increment its position and orientation in proportion to those forces, and find a new local equilibrium of the foam.

2.1. Forces on an ellipse

The ellipse is acted upon by three forces: (i) its weight mg, chosen sufficiently large that it will not come to rest during sedimentation; (ii) the resultant tension force $\vec{F}^n$ due to the network of films pulling it; (iii) the resultant pressure force $\vec{F}^p$ due to the pressure of the bubbles in contact with it. The films that are in contact with the ellipse are not uniformly distributed around its circumference – they bunch up at the trailing edge asymmetrically, see figure 1 – so that the resultant forces are usually non-zero. The network and pressure forces exerted on the ellipse both contribute towards the drag (upward) and lift (lateral) force it experiences, as well as the torque (rotation).

Each film i that meets the ellipse boundary does so at an angle of $\pi/2$ and contributes a force equal to the film tension 2γ on the object. We denote the position of the vertex at which the film meets the boundary by (x_i, y_i) and write $r_i = \sqrt{(x_i-x_0)^2+(y_i-y_0)^2}$ and $\tan\theta_i = (x_i-x_0)/(y_i-y_0)$. The force due to film i is directed at an angle α_i to the positive y direction, with

$$\tan\alpha_i = \frac{\left(1-e_c^4\right)\cos\phi\sin\phi\,(y_i-y_0)-\left(e_c^4\cos^2\phi+\sin^2\phi\right)(x_i-x_0)}{\left(1-e_c^4\right)\cos\phi\sin\phi\,(x_i-x_0)-\left(\cos^2\phi+e_c^4\sin^2\phi\right)(y_i-y_0)}\ . \tag{2}$$

The resultant network force is

$$\vec{F}^n = 2\gamma\sum_i\left(\sin\alpha_i,\cos\alpha_i\right)\ . \tag{3}$$

Since the vector describing the pull of each film does not go through the centre of the ellipse, the network force contributes to a torque that rotates the object. This network torque is dependent on the difference between the angles α_i and θ_i and is given by

$$\tau^n = 2\gamma \sum r_i \sin(\alpha_i - \theta_i), \tag{4}$$

with positive torque in the clockwise direction.

The pressure force exerted by the bubbles in contact with the ellipse is calculated in a similar way: a bubble k with pressure p_k that contacts the ellipse over a length l_k will exert a force in the inward normal direction, measured at the centrepoint of l_k, denoted (x_k, y_k). The length l_k is the arc length between the two vertices (x_i, y_i) and (x_{i+1}, y_{i+1}) at which the bubble meets the ellipse. The resultant pressure force is

$$\vec{F}^p = \sum_k p_k l_k (\sin\beta_k, \cos\beta_k) \tag{5}$$

where

$$\tan\beta_k = -\frac{y_{i+1} - y_i}{x_{i+1} - x_i}. \tag{6}$$

In addition, a non-zero pressure torque is exerted. As in the network force case, the amount of torque exerted depends on the difference between the angles β_k and θ_k. Thus, the torque exerted on the ellipse due to the pressure of the contacting bubbles is

$$\tau^p = \sum p_k l_k r_k \sin(\theta_k - \beta_k) \tag{7}$$

where $r_k = \sqrt{(x_k - x_0)^2 + (y_k - y_0)^2}$.

2.2. Fixed ellipse

We assume over-damped dynamics, with a time-scale set by either the drag on the bounding plates of the 2D experiment or by the frictional drag from the soap films that move around the perimeter of the ellipse; in both cases we assume that the torque is proportional to the angular velocity of the ellipse. Thus, a simulation iteration consists of moving the foam downstream by a small amount, taken as 2.1×10^{-3}, and changing the angle ϕ at which it is oriented by an amount:

$$\Delta\phi = \epsilon_0(\tau^n + \tau^p). \tag{8}$$

The constant ϵ_0 sets the effective time-scale for the rotational motion of the ellipse: as a result of the small magnitude of torque exerted on the ellipse we set $\epsilon_0 = 0.1$.

2.3. Sedimenting ellipse

The network and pressure contributions to the force exerted on an ellipse that has position $\vec{x}$ at a time t within the foam channel resist the gravity-driven motion. We again assume over-damped dynamics, so that the drag is proportional to the translational velocity of the ellipse. Thus, a simulation iteration consists of moving the ellipse centre point (x_0, y_0) by an amount $(\Delta x, \Delta y)$ and changing the angle ϕ at which it is oriented by an amount $\Delta\phi$:

$$\begin{aligned} \Delta x &= \epsilon_1(F_x^n + F_x^p) \\ \Delta y &= \epsilon_1(F_y^n + F_y^p + mg) \\ \Delta\phi &= \epsilon_2(\tau^n + \tau^p). \end{aligned} \tag{9}$$

To avoid numerical problems ϵ_1 must be smaller than the critical length l_c. We choose $\epsilon_1 = 3.6 \times 10^{-4}$, ensuring that the linear motion of the disc is slow enough that the assumptions of the quasistatic model are satisfied. We set $\epsilon_2 = 500\epsilon_1$ to avoid having to use unfeasibly long foam channels in order to observe the ellipse rotation. Thus in our simulations the ellipse is overly responsive to the torque applied on it during its sedimentation, but this work still provides qualitative evidence concerning the motion of the ellipse and the response of the foam.

3. Results

3.1. Fixed ellipse

3.1.1. Reference simulation

First we consider a reference simulation: the flow past a fixed ellipse of area ratio $a_r = A_e/A_b = 4$ and eccentricity $e_c = 0.8$, initially oriented with its major axis perpendicular to gravity, i.e. $\phi = 0$.

[Figure 2 here]

Figure 2(a) shows how the ellipse rotates into a stable orientation, $\phi = \pi/2$, that is, with its major axis parallel to the direction of gravity. The increase in the angle of orientation ϕ is initially very slow, suggesting that the orientation $\phi = 0$ is metastable and that the rotational motion is triggered by the disorder of the foam structure. Once the rotation of the ellipse has begun, there is a period of more rapid rotation until the major axis becomes parallel to the direction of gravity and only slight fluctuations in the orientation occur, indicating stability. We fit the orientation to the form

$$\phi(t) = \frac{\pi}{4}\left(1 + \tanh\left(s(t - t_0)\right)\right), \tag{10}$$

where t represents iteration number, with fitting parameters t_0 and

$$s = \frac{4}{\pi} \left. \frac{\mathrm{d}\phi}{\mathrm{d}t} \right|_{\phi=\pi/4}.$$

This assumes, as certainly seems appropriate in figure 2(a), that the rotation, and therefore the torque, is symmetric about $\phi = \pi/4$. The parameter s therefore allows us to estimate the maximum rotation rate of the ellipse.

The network and pressure contributions to the drag, lift and torque exerted on the ellipse are shown in figure 2 as a function of ϕ. There is an initial transient (not shown) lasting for about 50 iterations and the values show large fluctuations typical of very dry foams. The network contribution to the drag is significantly larger than the pressure contribution; both decrease towards the end of the motion, confirming the observation [15] that the drag force is dependent on the spanwise width of the ellipse and indicating that the drag is minimized when the ellipse is oriented such that its major axis is parallel to gravity. Both contributions to the lift are much smaller than the drag throughout but are maximized when the ellipse is oriented so that its major axis is far from being parallel or perpendicular to gravity. In this case the torque is negative, so that the ellipse rotates anticlockwise. Both the network and pressure forces contribute to the torque in the same sense; they are small when the ellipse is in either the metastable or stable orientations and the network contribution is greatest, as for the linear forces.

The rotation of the ellipse occurs due to the position of the films and the deformation of bubbles along its boundary. The films bunch up at the lowest point of the ellipse as the foam moves past it (figure 1). A slight fluctuation in the forces on the ellipse when it is oriented close to the metastable orientation results in films bunching up at an off-centre position on the ellipse boundary and therefore a non-zero network torque. Rotation of the ellipse continues until its highest point becomes its tip. Once the major axis of the ellipse is parallel to the y-direction the network torque applied by the films is minimized. The distribution and shape of the bubbles that surround the ellipse become less deformed when the ellipse is in this orientation. When the ellipse is oriented so that its major axis is perpendicular to gravity, bubbles in its wake are highly elongated and the bubbles at the leading edge are squeezed. However, when the ellipse is in its stable orientation, the deformation it causes to the foam is reduced.

The direction in which the ellipse rotates (clockwise or anticlockwise) is determined by the local structure of the foam. However, if the ellipse is placed close to one of the walls (data not shown) then the nearest wall determines the direction of rotation: more bubbles move from the front to the back of the ellipse on the side furthest from the wall, then films bunch close to the end of the ellipse closest to the wall and the network force causes it rotate. That is, it rotates anticlockwise close to the left-hand wall at $x = 0$ and clockwise close to the right-hand wall at $x = W$.

3.1.2. Validation

We attempt here to compare qualitatively our results with those of [15], who studied experimentally the slow flow of a monolayer of bubbles past an ellipse of area ratio 70 and eccentricity $e_c = 0.78$. The size of this ellipse is much higher than is possible in our simulations, but the eccentricity is similar. We show in figure 3 the drag, lift and torque on ellipses with $e_c = 0.8$ and $4 \leq a_r \leq 10$. All three increase in magnitude with the area of the ellipse. The drag shows the greatest dependence on area, and a linear decrease with orientation as in the experiment. The lift depends weakly on area, but again shows a response that is qualitatively similar to the experiment. The simulations correctly capture the shift towards higher ϕ in the torque, although it increases more smoothly with ϕ than in the experiment.

[Figure 3 here]

We consider the close correlation between our simulations for a fixed ellipse and the experiments to validate these simulations. We now turn to the sedimentation of an ellipse through a foam.

3.2. Sedimenting ellipse

3.2.1. Reference simulation

We again first consider a reference simulation: the sedimentation of the same reference ellipse as before ($a_r = 4$, $e_c = 0.8$) with weight $mg = 8$. Note that the weight is given a dimensionless value which is effectively the Bond number,

$$Bo = \frac{mg}{2\gamma a_r}. \tag{11}$$

The ellipse starts at a central position at the top of the foam and is initially oriented with its major axis perpendicular to gravity, i.e. $\phi = 0$.

[Figure 4 here]

The orientation ϕ increases in much the same way as for a fixed ellipse (figure 2(a)) during the descent, and the network and pressure contributions to the drag, lift and torque exerted on the ellipse are much as before (data not shown). The major axis again rotates until it becomes parallel to the direction of gravity. However, the ellipse also drifts laterally as it descends through the foam, as shown in figure 4(a), due to the non-zero component in the lift force when ϕ is far from both 0 and $\pi/2$.

[Figure 5 here]

To explain the foam's response to the sedimentation of an elliptical object, we show the fields of bubble displacement and pressure in figure 5. Instead of a symmetric bubble displacement field, bubbles move from the front to the back of the ellipse on only one side. The displacements are confined to within only a few bubble diameters of the ellipse (figure 6), indicating the screening [23] that the discrete nature of the foam causes. As the ellipse rotates, bubbles are squeezed in front and elongated at the back. Thus, a region of

high pressure exists in front of the object and on the side toward which it is rotating, while the wake consists of elongated bubbles of low pressure.

[Figure 6 here]

3.3. Varying ellipse area and eccentricity

The ellipse's eccentricity and area are varied independently, keeping all other parameters constant (including the weight, $mg = 8$). There is no clear trend in the time taken for the ellipse to leave the metastable orientation, since it depends upon the local disorder of the foam, but it is clear that each ellipse does rotate into the stable orientation. The variations in the magnitude of the ellipse orientation with iteration number are fitted to the form of eq. (10).

The results in figures 4(b) and 7 show that larger ellipses rotate more quickly, whether they are fixed or sedimenting. For example, the ellipse with $a_r = 10$, $e_c = 0.8$ has reached the stable orientation high up in the foam (figure 4(b)), and shows the greatest rotation rate (figure 7). This is due to a combination of factors: larger ellipses experience greater torque (figure 3(b)) because of the larger number of films that touch them, but in the case of sedimentation they descend more slowly because they are less dense (since the weight is fixed), giving more time for the rotation to occur.

[Figure 7 here]

Long, thin objects are expected to rotate at a greater rate than rounded objects, since films can bunch up at a position that is far from the object's centre of mass, resulting in a greater network torque being exerted by the foam. The deformation of the bubbles is also greater around a longer object. Note that in the absence of any viscous drag, as here, a circular disc experiences zero torque and would not rotate. The sedimentation of ellipses with eccentricities 0.70, 0.75, 0.80, 0.85, and 0.90, area $4A_b$ and weight 8, initially oriented with $\phi = 0$, is shown in figure 4(b). As expected, more eccentric ellipses rotate more quickly, summarized in figure 7.

4. Discussion

The sedimentation of an elliptical object in a dry 2D foam is a probe of foam rheology. An ellipse rotates to a stable orientation with its major axis parallel to the direction of gravity, independently of its initial orientation. A larger, more eccentric, ellipse rotates more quickly. The rotation is a result of the elasticity of the foam, modulated by its plasticity: it is driven by the bunching up of highly-stretched films in the wake of the ellipse at an off-centre position relative to the centre of mass of the ellipse, but when films become too close, T1 events occur and the driving force is lessened. The contribution of bubble pressures is less, but tends to act in the same sense as the network forces.

A further factor to be considered is the weight of the object, which we have chosen to be sufficient to allow downward motion without it becoming trapped (as would be the case for the reference case with an ellipse of half the weight). Heavier obstacles would descend more quickly, and the effect of the torque would be harder to observe, requiring much longer channels. Similarly, we expect that increasing the liquid fraction of the foam from the very small value used here would result in slower rotation, since the number of films that congregate at the highest point of the ellipse would be less. Incorporating viscous drag between the foam films and the sedimenting object would lead to greater network torques. Thus the required channel length would be reduced, making the calculations faster; however, introducing such a drag might increase the computational expense.

Acknowledgements

We thank K. Brakke for developing, distributing and supporting the Surface Evolver, and B. Dollet for generously providing experimental data. Financial support is gratefully acknowledged from EPSRC (EP/D071127/1).

References

[1] D. Weaire and S. Hutzler. The Physics of Foams, Oxford University Press, 2000.

[2] R. K. Prud'homme and S. A. Khan, editors. Foams: Theory, Measurements and Applications, CRC Press, 1996.

[3] J. J. Bikerman. Foams: Theory and Industrial Applications, Reinhold Publishing Corporation, New York, 1953.

[4] R. Höhler and S. Cohen-Addad. Topical review - rheology of liquid foam. J. Physics: Condensed Matter 17 (2005) R1041.

[5] G. G. Stokes. On the effect of the inertial friction of fluids on the motion of pendulums. Trans. Camb. Phil. Soc. IX (1850) 8.

[6] G. Boardman and R. L. Whitmore. Yield stress exerted on a body immersed in a Bingham fluid. Nature 187 (1960) 50.

[7] D. Rae. Yield stress exerted on a body immersed in a Bingham fluid. Nature 194 (1962) 272.

[8] P. Brunn. The slow motion of a rigid particle in a second-order fluid. J. Fluid Mech. 82 (1977) 529.

[9] L. G. Leal. The slow motion of slender rod-like particles in a second-order fluid. J. Fluid Mech. 69 (1975) 305.

[10] J. Wang and D. D. Joseph. Potential flow of a second-order fluid over a sphere or an ellipse. J. Fluid Mech. 511 (2004) 201.

[11] D. D. Joseph and J. Feng. A note on the forces that move particles in a second-order fluid. J. Non-Newtonian Fluid Mech. 64 (1996) 299.

[12] P. Y. Huang, J. Feng, and D. D. Joseph. The turning couples on an elliptic particle settling in a vertical channel. J. Fluid Mech. 271 (1994) 1.

[13] D. D. Joseph and Y. J. Liu. Orientation of long bodies falling in a viscoelastic liquid. J. Rheol. 37 (1993) 961.

[14] I. T. Davies and S. J. Cox. Sedimenting discs in a two-dimensional foam. Coll. Surf. A 344 (2009) 8.

[15] B. Dollet, M. Durth, and F. Graner. Flow of foam past an elliptical obstacle. Phys. Rev. E 73 (2006) 061404.

[16] B. Dollet, M. Aubouy, and F. Graner. Anti-inertial lift in foams: A signature of the elasticity of complex fluids. Phys. Rev. Lett. 95 (2005) 168303.

[17] K. Brakke. The Surface Evolver. Exp. Math. 1 (1992) 141.

[18] K. A. Brakke. 200,000,000 Random Voronoi Polygons. www.susqu.edu/brakke, 1986.

[19] I.T. Davies. Sedimentation of circular and elliptical objects in a two-dimensional foam. PhD thesis, Aberystwyth University, http://hdl.handle.net/2160/4179, 2009.

[20] C. Raufaste, B. Dollet, S. Cox, Y. Jiang, and F. Graner. Yield drag in a two-dimensional foam flow around a circular obstacle: Effect of liquid fraction. Euro. Phys. J. E. 23 (2007) 217.

[21] A. Wyn, I. T. Davies, and S. J. Cox. Simulations of two-dimensional foam rheology: Localization in linear Couette flow and the interaction of settling discs. Eur. Phys. J. E 26 (2008) 81.

[22] S. J.Cox, B. Dollet, and F. Graner. Foam flow around an obstacle: simulations of obstacle-wall interaction. Rheol. Acta. 45 (2006) 403.

[23] S. J. Cox, F. Graner, and M.F. Vaz. Screening in dry two-dimensional foams. Soft Matter 4 (2008) 1871.

Figure Captions

Figure 1: The films and bubbles in contact with the ellipse exert a network and pressure force on it. These contribute towards the drag, lift and torque exerted by the foam, and since they are distributed asymmetrically (the ellipse is sedimenting in the case shown, so that the films bunch up above it), the total contribution is usually non-zero.

Figure 2: (a) The orientation of a fixed ellipse of area $4A_b$ and eccentricity 0.8 changes so that the major axis is parallel to the direction of flow. The small variations about $\phi = \pi/2$ emphasises the stability of this orientation. Also shown is a fit to eq. (10). The network and pressure contributions to the (b) drag force, (c) lift force and (d) torque exerted on the same ellipse.

Figure 3: The (a) total drag and lift and (b) total torque on a fixed ellipse, for various areas. We choose to show lift and torque as negative, independent of the actual direction of rotation, to allow qualitative comparison with the experimental results of Dollet et al. [15] (in arbitrary units). Both drag and lift show the same shape: a linear decrease in drag and a quadratic dependence of lift on orientation. The torque is skewed towards larger orientations in both simulation and experiment, but the simulation does not show the sudden change in torque around $\phi = \pi/4$.

Figure 4: Tracking the ellipses as they descend through the foam shows that they drift laterally in the channel as they rotate towards a stable orientation. (a) An ellipse of area $4A_b$, eccentricity 0.8 and weight 8 sediments freely from an initial orientation in which its major axis is perpendicular to gravity ($\phi_{init} = 0$). The angle of orientation increases until the ellipse is oriented such that its major axis is parallel to gravity, which proves to be stable. Images of the ellipse are shown every 100 iterations. (b) The paths of ellipses of different sizes and eccentricities are shown with an outline of the ellipse either when it reaches the stable orientation (more eccentric, on the left, or larger, on the right) or when it reaches the bottom of the channel.

Figure 5: Measured fields for the reference simulation of figure 4(a). (a) Bubble displacement between the 250^{th} and the 280^{th} iteration. (b) Bubble pressures for the 250^{th} iteration. Dark gray denotes high pressure, light gray denotes low pressure.

Figure 6: The discrete nature of the foam causes the motion of the ellipse to be screened. The average displacement of each bubble is plotted as a function of the radial distance from the ellipse centre for the data of figure 5(a), each scaled by the bubble diameter. There is a clear drop in displacement beyond 4-5 bubble diameters from the ellipse.

Figure 7: The maximum rate of rotation calculated from the slope of the fit to eq. (10) for a range of ellipse eccentricities (lines of negative slope, lower axis) and areas (lines of positive slope, upper axis). Data for fixed and sedimenting ellipses are very similar. The rotation rate increases as the ellipse becomes larger

and/or more eccentric.

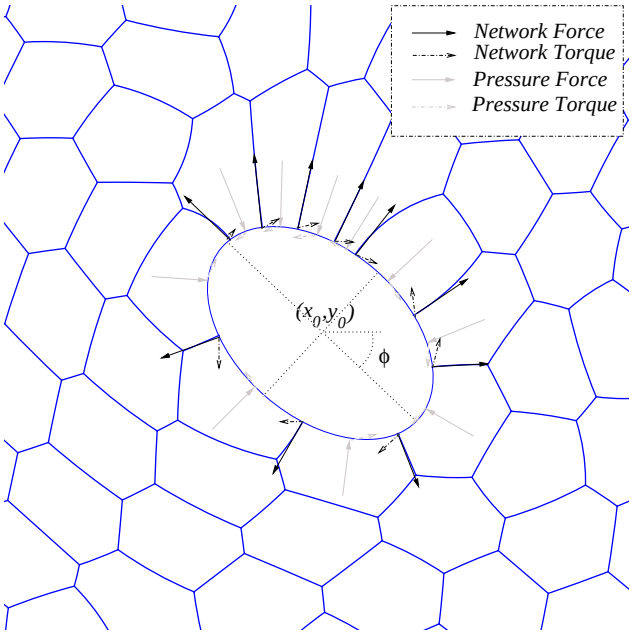

Figure 1: The films and bubbles in contact with the ellipse exert a network and pressure force on it. These contribute towards the drag, lift and torque exerted by the foam, and since they are distributed asymmetrically (the ellipse is sedimenting in the case shown, so that the films bunch up above it), the total contribution is usually non-zero.

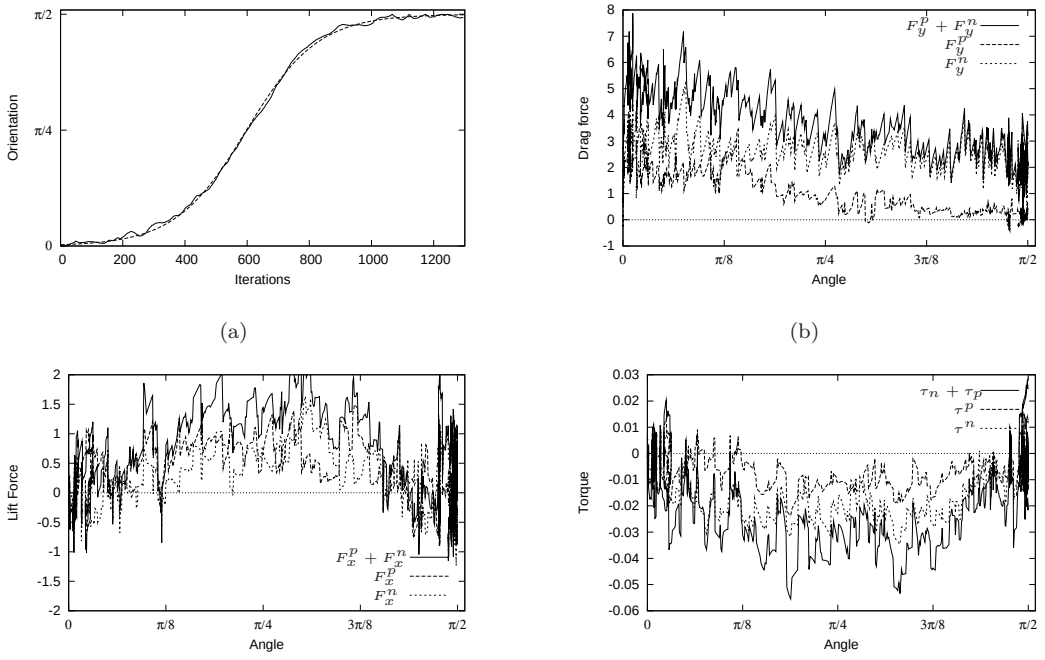

Figure 2: (a) The orientation of a fixed ellipse of area $4A_b$ and eccentricity 0.8 changes so that the major axis is parallel to the direction of flow. The small variations about $\phi = \pi/2$ emphasises the stability of this orientation. Also shown is a fit to eq. (10). The network and pressure contributions to the (b) drag force, (c) lift force and (d) torque exerted on the same ellipse.

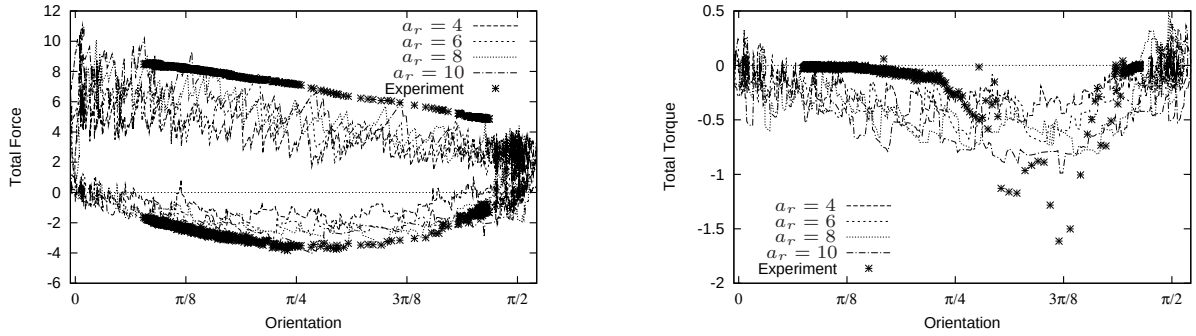

(a) (b)

Figure 3: The (a) total drag and lift and (b) total torque on a fixed ellipse, for various areas. We choose to show lift and torque as negative, independent of the actual direction of rotation, to allow qualitative comparison with the experimental results of Dollet et al. [15] (in arbitrary units). Both drag and lift show the same shape: a linear decrease in drag and a quadratic dependence of lift on orientation. The torque is skewed towards larger orientations in both simulation and experiment, but the simulation does not show the sudden change in torque around $\phi = \pi/4$.

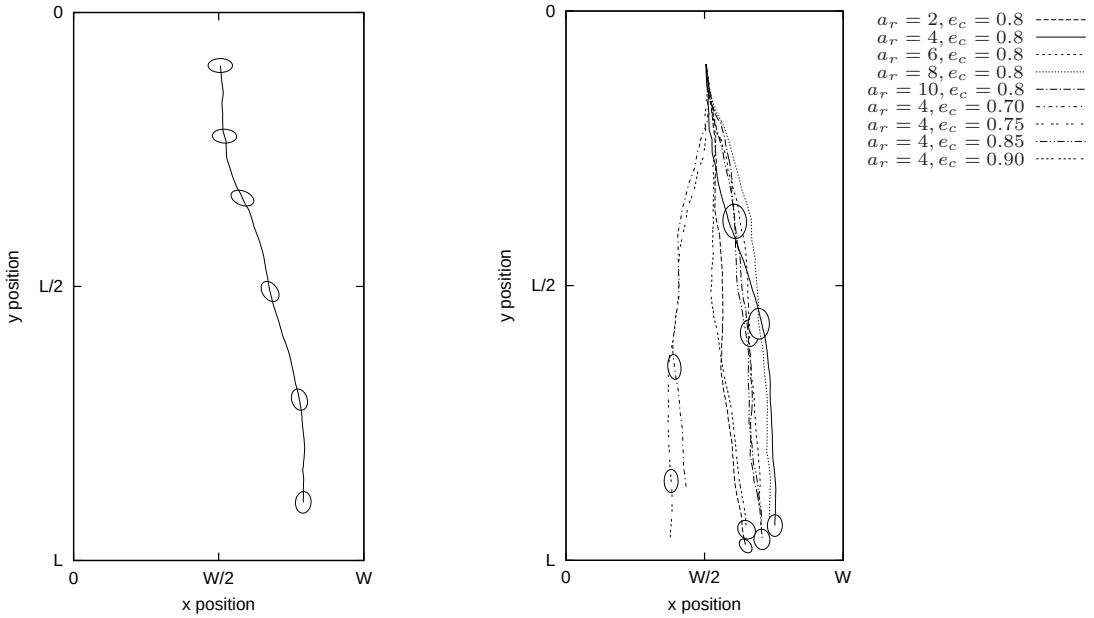

(a) (b)

Figure 4: Tracking the ellipses as they descend through the foam shows that they drift laterally in the channel as they rotate towards a stable orientation. (a) An ellipse of area $4A_b$, eccentricity 0.8 and weight 8 sediments freely from an initial orientation in which its major axis is perpendicular to gravity ($\phi_{init} = 0$). The angle of orientation increases until the ellipse is oriented such that its major axis is parallel to gravity, which proves to be stable. Images of the ellipse are shown every 100 iterations. (b) The paths of ellipses of different sizes and eccentricities are shown with an outline of the ellipse either when it reaches the stable orientation (more eccentric, on the left, or larger, on the right) or when it reaches the bottom of the channel.

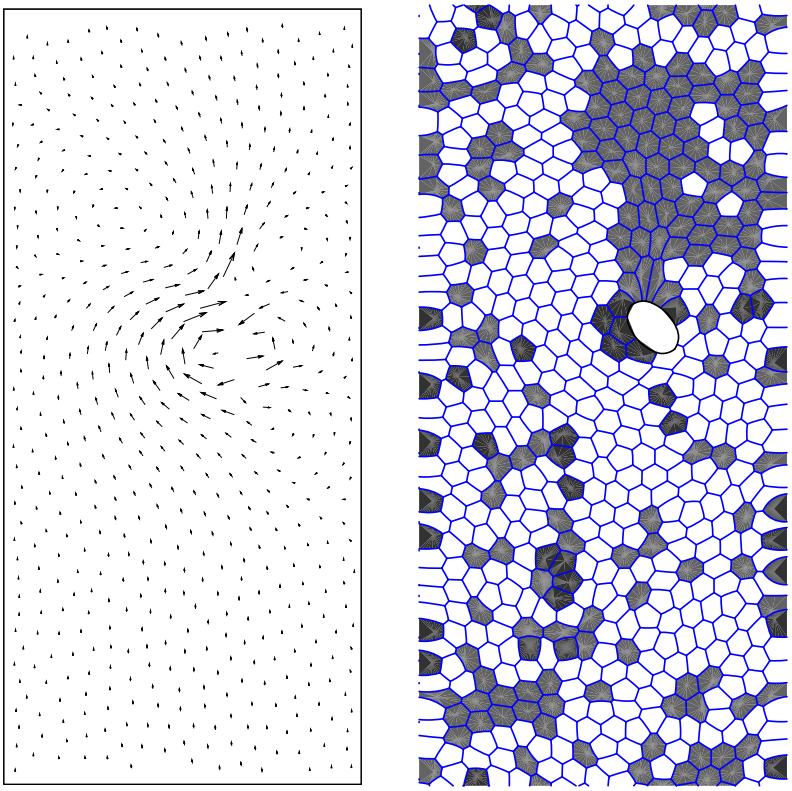

Figure 5: Measured fields for the reference simulation of figure 4(a). (a) Bubble displacement between the 250^{th} and the 280^{th} iteration. (b) Bubble pressures for the 250^{th} iteration. Dark gray denotes high pressure, light gray denotes low pressure.

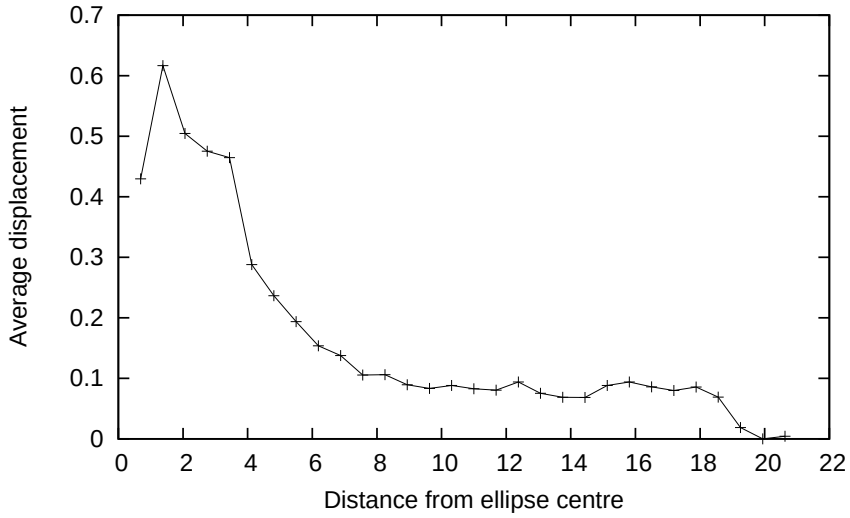

Figure 6: The discrete nature of the foam causes the motion of the ellipse to be screened. The average displacement of each bubble is plotted as a function of the radial distance from the ellipse centre for the data of figure 5(a), each scaled by the bubble diameter. There is a clear drop in displacement beyond 4-5 bubble diameters from the ellipse.

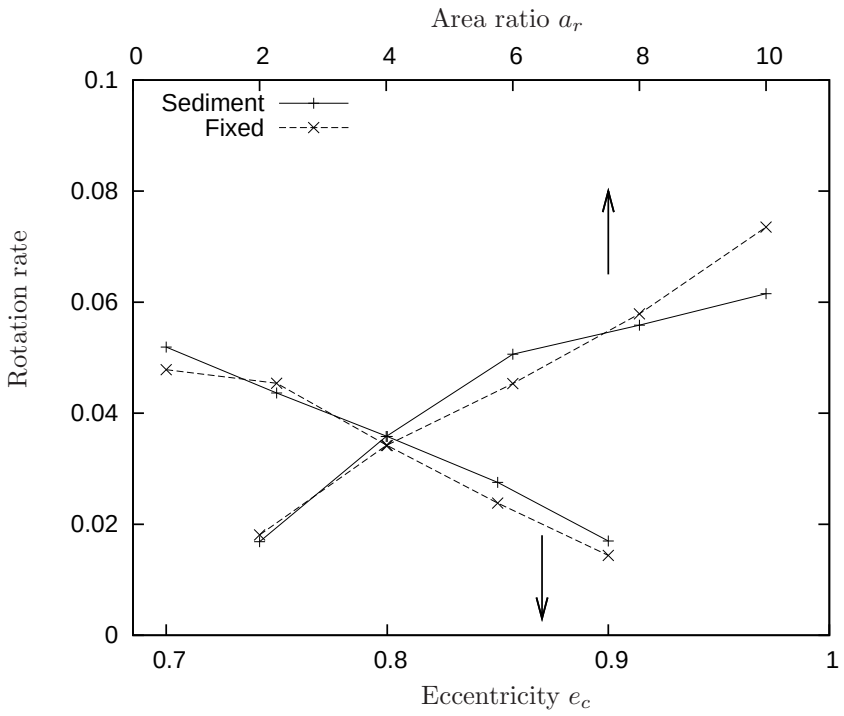

Figure 7: The maximum rate of rotation calculated from the slope of the fit to eq. (10) for a range of ellipse eccentricities (lines of negative slope, lower axis) and areas (lines of positive slope, upper axis). Data for fixed and sedimenting ellipses are very similar. The rotation rate increases as the ellipse becomes larger and/or more eccentric.